Supplemental - Evidence for microbial mediated nitrate cycling within floodplain sediments during groundwater fluctuations

Nicholas J Bouskill[1], Mark E Conrad[1], Markus Bill[1], Eoin L Brodie[1], Yiwei Cheng[1], Chad Hobson[1], Matthew Forbes[2], Karen L Casiotti[2], and Kenneth H Williams[1]

[1]Earth and Environmental Sciences Area, Lawrence Berkeley National Laboratory, Berkeley, CA, 94720
[2]Department of Environmental Earth System Science, Stanford University, Stanford, CA, 94305

Correspondence to: Nicholas Bouskill (njbouskill@lbl.gov)

1 Supplemental Methods

1.1 Fraction of nitrate formed by nitrification

A simple isotope mixing model (Wexler et al., 2014) was used to estimate the contribution of different sources (i.e., NO_3^- deposition and infiltration or nitrification) to NO_3^- accumulating in the unsaturated zone prior to groundwater rise. Using literature values for two different end members (nitrification and snowmelt) we estimated the source of well NO_3^- prior to the onset of denitrification (toward the beginning of May) as follows,

$$Well\ \delta^{18}O_{NO_3} = f * Snow\ \delta^{18}O_{NO_3} + (1-f) Nitrif\ \delta^{18}O_{NO_3} \tag{1}$$

which can be rearranged to give *f*,

$$f = \frac{(Well\ \delta^{18}O_{NO_3} - Nitrif\ \delta^{18}O_{NO_3})}{(Snow\ \delta^{18}O_{NO_3} - Nitrif\ \delta^{18}O_{NO_3})} \tag{2}$$

Values for $\delta^{18}O_{NO_3}$ from snowmelt were taken from previously published values (Campbell et al., 2002; Kendall et al., 2007), estimated to be $\sim$ +67 ‰ (with a range of +40 to +70 ‰). Two approaches were taken to estimate the $\delta^{18}O_{NO_3}$ imparted by nitrification (Fang et al., 2012). The first approach follows the assumption that nitrification occurs with no exchange between nitrification intermediates and water, though isotopic fractionation during oxygen atom incorporation is accounted for (Buchwald et al., 2012):

$$\delta^{18}O_{NO_3} = \frac{2}{3}\delta^{18}O_{H_2O} + \frac{1}{3}\delta^{18}O_{O_2} - \frac{1}{3}\left({}^{18}\varepsilon_{K,O_2} + {}^{18}\varepsilon_{K,H_2O,1} + {}^{18}\varepsilon_{K,H_2O,2}\right) \tag{3}$$

Here we used a fixed value of 23.5 ‰ for the $\delta^{18}O_{O_2}$, and measurements from the Rifle groundwater where $\delta^{18}O_{H_2O}$ spans a range of -13.3 to -14.7 ‰ between the 2 and 3 m depths considered in this study (Ken Williams, pers. comm). ${}^{18}\varepsilon_{K,O_2}$ and

$^{18}\varepsilon_{K,H_2O,1}$ represents the isotopic fractionation associated with ^{18}O incorporation from O_2, and H_2O during the first step of nitrification, ammonia oxidation. Similarly, $^{18}\varepsilon_{K,H_2O,2}$ represent the isotopic fractionation associated with ^{18}O incorporation into NO_3 from H_2O during nitrite oxidation. Values for $^{18}\varepsilon_{K,O_2}$, $^{18}\varepsilon_{K,H_2O,1}$, and $^{18}\varepsilon_{K,H_2O,2}$ were derived from a previously published range of values (Buchwald and Casciotti, 2010; Casciotti et al., 2010), where $^{18}\varepsilon_{K,O_2}$ + $^{18}\varepsilon_{K,H_2O,1}$ was estimated as -37.6 to -17.9 ‰ (Casciotti et al., 2010), while $^{18}\varepsilon_{K,H_2O,2}$ has been estimated to be -18.2 to -12.8 ‰ (Buchwald and Casciotti, 2010). The range of nitrification $\delta^{18}O_{NO_3}$ values obtained through this first approach is -20.3 to -11.2. ‰.

The second approach allows full exchange of oxygen atoms between NO_2^- and H_2O during nitrification (Buchwald and Casciotti, 2010; Casciotti et al., 2010; Buchwald et al., 2012):

$$\delta^{18}O_{NO_3} = \delta^{18}O_{H_2O} + \frac{2}{3}(^{18}\varepsilon_{eq}) - \frac{1}{3}(^{18}\varepsilon_{K,H_2O,2}) \quad (4)$$

where $^{18}\varepsilon_{eq}$ is the equilibrium isotope effect between NO_2^- and H_2O, which is approximately 14-15 ‰ at room temperature (Casciotti et al., 2007; Buchwald and Casciotti, 2013). The range of nitrification $\delta^{18}O_{NO_3}$ values obtained through this second approach is -11.5 to -7.7 ‰.

1.2 Model Description

To further understand the factors controlling rates of nitrogen cycling and nitrogen loss from the Rifle aquifer, we represent an ecosystem of interacting functional microbial guilds competing for carbon and nitrogen in a manner theoretically analogous to the R* concept (Tilman, 1977; 1987). The different microbial guilds represent facultative heterotrophs (denitifiers), and obligate and mixotrophic autotrophs (aerobic and anaerobic ammonia-oxidizing organisms and nitrite-oxidizing bacteria, Figure S1). The model framework is based on a previously published trait-based model of nitrification (Bouskill et al., 2012; Le Roux et al., 2016), with several modifications: (1) the present model develops this earlier structure through the representation of functional guilds (defined here as discrete collection of organisms performing a common metabolism) as ecological strategies that encompass a variance in trait space rather than representing specific phylogenetic groups. This reduces the complexity of certain functional guilds from previous representations. For example, the ammonia-oxidizing organisms have been reduced to four functional guilds from the 8 established previously (Bouskill et al., 2012). (2) Improved representation of the nitrite oxidizing bacteria encompassing both obligate autotrophic and mixotrophic metabolisms. The rationale for which has been described previously (Le Roux et al., 2016). (3) Inclusion of thermodynamically driven heterotrophic reactions based on previously published work (LaRowe and Van Cappellen, 2011; LaRowe et al., 2012), where the electron donor and acceptor pairing determines energy production (i.e., ATP equivalents) and growth rates (see below). (4) Representation of the anaerobic ammonia oxidizing (anammox) planctomycetes, with trait ranges derived from recently published ecophysiological data (Kartal et al., 2011).

Heterotrophic functional guilds: The heterotrophs are represented by four distinct guilds that include three facultative aerobes with the metabolic flexibility to switch from respiration via oxygen (O_2) as an electron acceptor, to nitrate (NO_3^-). Two of these guilds catalyze complete denitrification pathways (i.e., from NO_3^- to N_2), but differ in their affinity (K_M) for

O_2 and NO_3^-, while the third guild mediates only partial denitrification to N_2O rather than N_2. The final guild is an obligate anaerobe and N_2O consumer (Jones et al., 2014; Sanford et al., 2012) reducing N_2O to N_2.

Within each guild there are three ecotypes that couple different electron acceptors (either O_2 or NO_3^-) to one of three different electron donors (ED 1, 2, 3). These electron donors differ in their C:N ratios, on the basis of measurements made at the Rifle site (C:N = 5, 11, 15,), and their thermodynamic activity coefficients (k_{eq}, table S2). The three ecotypes are parameterized as diverse ecological strategies, and differ in their capabilities to utilize the ED_{1-3}. Ecotype 1 specializes on one compound only (ED_1, C:N = 5), with no capacity to take up ED_2 or ED_3. By contrast ecotype 3 can utilize all three different electron donors, and ecotype 2 showing an intermediate strategy, utilizing ED_1 and ED_2 (C:N = 11). Physiological trade-offs constrain the metabolically diverse ecotypes to specific regions of the trait-space because the capacity to take-up and utilize multiple donor sources trades-off against growth rate. Consequentially, specialists have a higher maximal growth rate relative to the other two ecotypes, while the generalist has a lower growth rate. The heterotrophic functional guilds also conform to the general trade-off rules specified below. The rate of nitrogen loss and nitrous oxide (N_2O) production is dependent on multiple interacting factors, including, microbial community structure, nitrification rate, nutrient concentrations, organic matter stoichiometry, redox conditions and temperature (Groffman, 2012; Wallenstein et al., 2006). Trait values are given in Table S1, and are derived from previously published literature values in an attempt to span trait variance and represent different ecological strategies.

1.2.1 Carbon and nutrient cycling

The three ED pools have different chemical structures (represented with different thermodynamic equilibrium constants, see table S2) and different C:N stoichiometries (5 - 15). Heterotrophic mineralization of substrate pools yields ammonia (NH_3^+) that, under aerobic conditions, can be nitrified to NO_2^- and then to NO_3^- via ammonia- and nitrite-oxidizing organisms. Under aerobic unsaturated conditions in the aquifer, NO_3^- builds up. The substrate and nutrient dynamics are represented as follows,

$$\frac{dED}{dt} = \sum_j m.B_{i,j} - \sum_j U\big(ED, B_{i,j}, T\big) \tag{5}$$

$$\frac{dN}{dt} = \sum_j m.B_{i,j} - \sum_j U\big(N, B_{i,j}T\big) \tag{6}$$

where, ED and N represent the concentration (in M) of the electron donors and nutrients, respectively. U represents uptake by different functional guilds (kinetics outlined below), and T is the temperature (C). The initial inputs are the concentration of electron donor ($ED_{1,2,3}$), and oxygen concentrations. These values are prescribed in the model on the basis of measured organic matter fractions and oxygen concentrations within the Rifle aquifer.

1.2.2 Microbial physiology and nutrient uptake

Below we describe the equations determining resource uptake and utilization for heterotrophic organisms and anaerobic ammonium oxidation. The relevant equations for the AOO and NOB uptake and growth have been described previously (Bouskill et al., 2012; Le Roux et al., 2016). Microbial biomass dynamics are governed by substrate and nutrient uptake, resulting in biomass development, and balanced by a first order mortality rate, according the following,

$$\frac{d_B}{dT} = d_B - m \cdot B_T^i \tag{7}$$

where, d_B represents biomass development through cell division (equation 9), and m represents a biomass dependent (B_T) mortality rate. The exception to this relationship occurs during detoxification of NO_2 by ammonia-oxidizers, which uses biomass as the energy source to oxidize NO_2 via a series of intermediates (NO and N_2O)(Bouskill et al., 2012). The detoxification term modifies the biomass dynamics as follows,

$$\frac{dB}{dT} = D_B - m \cdot B_T^i - \frac{1}{4}\left(l_{DETOX}^{NO_2} + l_{DETOX}^{NO}\right) \tag{8}$$

where, l_{DETOX} (Ms^{-1}) represents the loss of biomass due to the detoxification of either NO_2 or NO. The $\frac{1}{4}$ represents the stoichiometric relationship between AOB biomass loss and NO_2. NO is detoxified to N_2O and is the dominant pathway via which nitrifiers contribute to the N_2O production. The decomposition of hydroxylamine (NH_2OH) is a second pathway through which ammonia-oxidiers produce N_2O, however, this is likely of secondary important to total N_2O flux (Bouskill et al., 2012). The rate of microbial cell division (D_B) can then be given by,

$$d_B = \mu_{MAX}^B \cdot min\left(d_i\right) \cdot B_T \tag{9}$$

where, μ_{MAX}^B represents the maximum growth rate (s^{-1}) of the members of the different function guilds, and B_T represents the total microbial biomass, which is dependent on the rate of resource utilization.

1.3 Resource utilization

Here, the uptake of different substrates and electron acceptors is represented using Michaelis Menton (MM) kinetics, which have been conventionally employed to represent resource uptake by bacteria (Litchman et al., 2015).

Anaerobic ammonia oxidizers: The uptake of NH_4 and NO_2 by anammox bacteria follows a dual MM expression with inhibition by O_2:

$$V^{NH_4} = V_{MAX}^{NH_4} \cdot \frac{[NH_4]}{K_{NH_4}^M + [NH_4]} \cdot \frac{[O_2]}{K_{O_2}^i + [O_2]} \tag{10}$$

where $V_{MAX}^{NH_4}$ represents the maximum uptake rate for NH_4, $K_M^{NH_4}$ represents the affinity constant for NH_4 and $K_i^{O_2}$ represents the inhibition constant for O_2.

From this, the uptake of NO_2 is calculated according to the stoichiometric ratio of the anammox reaction,

$$1NH_4 + 1.3NO_2 \longrightarrow 1N_2 + 0.3NO_3 + 2H_2O \tag{11}$$

The anammox bacteria maintain a stoichiometric C:N ratio (= 6.6) through the uptake and assimilation of N (as NH_4) into biomass, according to,

$$V^N = V_{MAX}^N \cdot \frac{[N]}{K_M^N + [N]} \tag{12}$$

Finally, anammox increase biomass (eq. 8) via carbon fixation using energy generated through ammonia oxidation. CO_2 uptake proceeds according to,

$$V^{CO_2} = V_{MAX}^N \cdot \frac{[CO_2]}{K_M^{CO_2} + [CO_2]} \tag{13}$$

Facultative heterotrophs: Heterotrophic respiration rates are calculated according to the following,

$$r_R = V_{MAX} \cdot [B_{j,t}] \cdot f(ED) \cdot f(EA) \cdot f(T) \tag{14}$$

where, V_{MAX} is the maximum uptake rate for either the ED or EA, f(ED) and f(EA) are MM functions for each ED and EA (i.e., O_2, NO_3), and f(T) represents the thermodynamic potential, which is a dimensionless thermodynamic potential factor. The f(T) function constrains the microbial respiration rate based on differences between the available energy from the environment (i.e., coupled ED and EA) and a minimum amount of energy harvested by microbial cells for growth and maintenance (ΔG_{min}). The formulation of f(T) in recent years, illustrated the increasing recognition of the need of a more robust method to model microbial respiration rates, which are typically constrained by low energy availability[9,17]. At present, two formulations of f(T) that differ in the proxy used to represent ΔG_{min} are commonly used (Jin and Bethke, 2007; LaRowe et al., 2012). For example, Jin and Bethke (Jin and Bethke, 2007) represent ΔG_{min} by the energetics of ATP synthesis by microorganisms, while LaRowe and coworkers (LaRowe et al., 2012) proposed ΔG_{min} be represented by the energetics of microbial membrane potential. In the current model, the f(T) formulation of LaRowe et al (LaRowe et al., 2012) has been implemented,

$$f(T) = \frac{1}{e^{\left(\frac{\Delta G_r + F\Delta\psi}{RT}\right)} + 1} \tag{15}$$

where, $\Delta\psi$ is the membrane potential, which is set here at a value optimal for ATP production (120 mV, (LaRowe et al., 2012), R is the gas constant (8.314 J mol^{-1} K^{-1}), T is temperature in Kelvin, and F is Faraday's constant (96485.34 C mol^{-1}). ΔG_r is the Gibbs free energy of the redox reaction per electron transferred, and is calculated as:

$$\Delta G_r = -RTln\left(\frac{K}{Q}\right) \tag{16}$$

where K is the reaction equilibrium constant while Q is the reaction quotient of the same reaction. Q is derived as,

$$Q = \prod_i a_i^{v_i} \tag{17}$$

where, a_i and v_i are the activity coefficient (mol l^{-1}) and the stoichiometric coefficient of chemical species (i) in the redox reaction.

Temperature response: We assume that the microorganisms within the aquifer are adapted to the average annual temperature within the TT-03 well (mean $\pm$ std dev = 13.5 $\pm$ 0.8 °C). The temperature response is then represented using a previously published function that fixes the shape of the specific activity of a transporter or enzyme as a gaussian distribution across a gradient of temperature (Rosso et al., 1995).

1.3.1 Trade-offs

Metabolic trade offs are key in determining the relative fitness of individual cells across gradients and the evolution of the microbial community (Beardmore et al., 2012; Edwards et al., 2013). In the present model we represent several hardwired trade-offs that may constrain metabolism.

Affinity uptake trade-off: A negative relationship has been observed between the maximal rate of substrate uptake (V_{MAX}) and the uptake affinity (V_{MAX}/ K_M) (Button et al., 2004). While the precise shape of this trade-off is currently unclear, in the present model we represent a tentative linear relationship between these two traits. This relationship is predominantly used for distinguishing different heterotrophic organisms (from oligo- to copiotrophic bacteria), where the organisms are differentiated on the basis of substrate affinity and uptake. These traits are generally standardized across the other guilds.

Growth-rate physiological efficiency trade-off: Microbial CUE is a non-linear and hysteretic trait (Tang and Riley, 2014), that varies as a function of temperature and mineral interactions. However, to reduce the complexity associated with this trait, we parameterize it as a static value related to the growth rate of different microbial guilds and modified by temperature. In the present model we represent fast growing heterotrophic organisms as metabolically inefficient, with a lower CUE and associated greater production of CO_2/ unit C taken up (Molenaar et al., 2009). Slow growing organisms, however, partition more carbon (either fixed or taken up from the soil) to the biomass rather than to maintenance.

Code availability: Scripts used in the current simulations are available online (www.njbouskill.wordpress.com/codes).

2 References

Beardmore, R. E., Gudelj, I., Lipson, D. A. and Hurst, L. D.: Metabolic trade-offs and the maintenance of the fittest and the flattest. Nature, 472(7343), 342-346, doi:10.1038/nature09905, 2012.

Bouskill, N. J., Tang, J., Riley, W. J. and Brodie, E. L.: Trait-based representation of biological nitrification: model development, testing, and predicted community composition. Front. Microbiol., 3, 364, doi:10.3389/fmicb.2012.00364, 2012.

Buchwald, C. and Casciotti, K. L.: Oxygen isotopic fractionation and exchange during bacterial nitrite oxidation. Limnol. Oceangr., 55(3), 1064-1074, doi:10.4319/lo.2010.55.3.1064, 2010.

Button, D. K., Robertson, B., Gustafson, E. and Zhao, X.: Experimental and Theoretical Bases of Specific Affinity, a Cytoarchitecture-Based Formulation of Nutrient Collection Proposed To Supercede the Michaelis-Menten Paradigm of Microbial Kinetics. Applied and Environmental Microbiology, 70(9), 5511-5521, doi:10.1128/AEM.70.9.5511-5521.2004, 2004.

Casciotti, K. L., McIlvin, M. and Buchwald, C.: Oxygen isotopic exchange and fractionation during bacterial ammonia oxidation. Limnol. Oceangr., 55(2), 753, 2010.

Edwards, K. F., Klausmeier, C. A. and Litchman, E.: A Three-Way Trade-Off Maintains Functional Diversity under Variable Resource Supply. Am. Nat., 182(6), 786-800, doi:10.1086/673532, 2013.

Fang, Y., Koba, K., Makabe, A., Zhu, F., Fan, S., Liu, X. and Yoh, M.: Low $^{1}8$O Values of Nitrate Produced from Nitrification in Temperate Forest Soils. Environ. Sci. Technol., 46(16), 8723-8730, doi:10.1021/es300510r, 2012.

Groffman, P. M.: Terrestrial denitrification: challenges and opportunities. Ecological Processes, 1(1), 1-11, 2012.

Jin, Q. and Bethke, C. M.: The thermodynamics and kinetics of microbial metabolism. American Journal of Science, 307(4), 643-677, doi:10.2475/04.2007.01, 2007.

Jones, C. M., Spor, A., Brennan, F. P., Breuil, M.-C., Bru, D., Lemanceau, P., Griffiths, B., Hallin, S. and Philippot, L.: Recently identified microbial guild mediates soil N2O sink capacity. Nature Climate Change, doi:10.1038/nclimate2301, 2014.

Kartal, B., Geerts, W. and Jetten, M. S.: 4 Cultivation, Detection, and Ecophysiology of Anaerobic Ammonium-Oxidizing Bacteria. Meth. Enzymol., 486 (Part A), 89-108, doi:10.1016/S0076-6879(11)86004-0, 2011.

Kendall, C., Elliott, E. M. and Wankel, S. D.: Tracing anthropogenic inputs of nitrogen to ecosystems. Stable isotopes in ecology, 2007.

LaRowe, D. E. and Van Cappellen, P.: Degradation of natural organic matter: A thermodynamic analysis. Geochimica et Cosmochimica Acta, 75(8), 2030-2042, doi:10.1016/j.gca.2011.01.020, 2011.

LaRowe, D. E., Dale, A. W., Amend, J. P. and Van Cappellen, P.: Thermodynamic limitations on microbially catalyzed reaction rates. Geochimica et Cosmochimica Acta, 90, 96-109, doi:10.1016/j.gca.2012.05.011, 2012.

Le Roux, X., Bouskill, N. J., Niboyet, A., Barthes, L., Dijkstra, P., Field, C. B., Hungate, B. A., Lerondelle, C., Pommier, T., Tang, J., Terada, A., Tourna, M. and Poly, F.: Predicting the Responses of Soil Nitrite-Oxidizers to Multi-Factorial Global Change: A Trait-Based Approach. Front. Microbiol., 7, doi:10.3389/fmicb.2016.00628, 2016.

Litchman, E., Edwards, K. F. and Klausmeier, C. A.: Microbial resource utilization traits and trade-offs: implications for community structure, functioning, and biogeochemical impacts at present and in the future. Front. Microbiol., 6(e32003), 65, doi:10.3389/fmicb.2015.00254, 2015.

Molenaar, D., van Berlo, R., de Ridder, D. and Teusink, B.: Shifts in growth strategies reflect tradeoffs in cellular economics. Mol Syst Biol, 5, doi:10.1038/msb.2009.82, 2009.

Rosso, L., Lobry, J. R., Bajard, S. and Flandrois, J. P.: Convenient Model To Describe the Combined Effects of Temperature and pH on Microbial Growth. Applied and Environmental Microbiology, 61(2), 610-616, 1995.

Sanford, R. A., Wagner, D. D., Wu, Q., Chee-Sanford, J. C., Thomas, S. H., Cruz-Garcia, C., Rodriguez, G., Massol-Deya, A., Krishnani, K. K., Ritalahti, K. M., Nissen, S., Konstantinidis, K. T. and Loffler, F. E.: Unexpected nondenitrifier nitrous oxide reductase gene diversity and abundance in soils. Proc. Natl. Acad. Sci. U.S.A., 109(48), 19709-19714, doi:10.1073/pnas.1211238109, 2012.

Tang, J. and Riley, W. J.: Weaker soil carbon-climate feedbacks resulting from microbial and abiotic interactions. Nature Climate Change, doi:10.1038/nclimate2438, 2014.

Tilman, D.: Resource competition between plankton algae: an experimental and theoretical approach. Ecology, 338-348, 1977.

Tilman, D.: Further thoughts on competition for essential resources. Theoretical Population Biology, 32(3), 442-446, 1987.

Wallenstein, M. D., Myrold, D. D., Firestone, M. and Voytek, M.: Environmental controls on denitrifying communities and denitrification rates: insights from molecular methods. Ecol Appl, 16(6), 2143-2152, 2006.

Wexler, S. K., Goodale, C. L., McGuire, K. J., Bailey, S. W. and Groffman, P. M.: Isotopic signals of summer denitrification in a northern hardwood forested catchment. Proc. Natl. Acad. Sci. U.S.A., 111(46), 16413-16418, doi:10.1073/pnas.1404321111, 2014.

3 Supplemental Tables and Figures

Functional Guild	Trait															
	Resource acquisition															
	Growth rate	Oxygen		Ammonium	Nitrate	Nitrous oxide	ED1			ED2			ED3			
	μ_{MAX} (d^{-1}) /3600	K_M (M) *$1x10^{-6}$	K_i (M) *$1x10^{-6}$	K_M (M) *$1x10^{-5}$	K_M (M) *$1x10^{-6}$	K_M (M) *$1x10^{-6}$	K_M (M) *$1x10^{-6}$	V_{MAX} (d^{-1}) *$1x10^{-6}$	Yld	K_M (M) *$1x10^{-6}$	V_{MAX} (d^{-1}) *$1x10^{-6}$	Yld	K_M (M) *$1x10^{-6}$	V_{MAX} (d^{-1}) *$1x10^{-6}$	Yld	Stoichiometry (min)
Facultative (NO2 -> N2)																
H1 - Specialist	8	0.5	1	1	100	-	50	28	0.035	-	-	-	-	-	-	5
H2 - Intermediate	5.5	0.5	1	1	100	-	250	15	0.045	50	10	0.025	-	-	-	5
H3 - Generalist	2.5	0.5	1	1	100	-	500	8	0.055	100	5	0.035	100	10	0.035	5
Facultative (NO2 -> N2)																
H4 - Specialist	6	5	0.1	1	10	-	50	20	0.045	-	-	-	-	-	-	5
H5 - Intermediate	4	5	0.1	1	10	-	250	10	0.055	50	10	0.035	-	-	-	5
H6 - Generalist	1	5	0.1	1	10	-	500	5	0.065	100	5	0.045	100	10	0.05	5
Facultative (NO2 -> N2O)																
H7 - Specialist	7	5	0.1	1	10	-	50	21	0.042	-	-	-	-	-	-	5
H8 - Intermediate	5	5	0.1	1	10	-	250	12	0.052	50	10	0.03	-	-	-	5
H9 - Generalist	2	5	0.1	1	10	-	500	7	0.062	100	5	0.04	100	10	0.04	5
Obligate (N2O -> N2)																
H10 - Specialist	4	-	0.1	1	10	10	50	20	0.04	-	-	-	-	-	-	5
H11 - Intermediate	0.8	-	0.1	1	10	50	250	10	0.05	50	10	0.03	-	-	-	5
H12 - Generalist	0.3	-	0.1	1	10	100	500	5	0.06	100	5	0.04	100	10	0.05	5

Table S1. Heterotrophic guild trait values representing the different ecological strategies represented in the model. Parameter values were extracted from previous publications (see supplemental materials).

	Trait Resource acquisition												
Functional Guild	**Growth rate**	**Ammonium/ Nitrite**			**Nitrite**			**Carbon Dioxide**	**Oxygen**		**Stoichiometry**	**Yld**	**References**
	μ_{MAX} (d^{-1}) /3600	K_M (M) *$1x10^{-6}$	V_{MAX} (d^{-1}) *$1x10^{-6}$	K_I (M) *$1x10^{-6}$	K_M (M) *$1x10^{-6}$	V_{MAX} (d^{-1}) *$1x10^{-6}$	K_I (M) *$1x10^{-6}$	K_M (M) *$1x10^{-6}$	K_M (M) *$1x10^{-6}$	K_I (M) *$1x10^{-7}$	CN	/CN	
Ammonia-oxidation													
AOB_1	0.9	200	10	-	-	-	-	1	3	-	6.6	0.04	See Bouskill et al., 2012 for list of sources
AOB_2	0.8	100	7	-	-	-	-	1	3	-	6.6	0.045	
AOB_3	0.3	40	2	-	-	-	-	1	3	-	6.6	0.05	
AOA_1	0.25	0.05	1.7	100	-	-	-	1	3	-	6.6	0.06	
Nitrite-oxidation													
NOB_1	0.7	100	-	-	349	6	-	1	8		6.6	0.04	Le Roux et al., 2016
NOB_2	0.5	100	-	-	1035	8	-	1	10		6.6	0.04	
NOB_3	0.3	100	-	-	19	2	-	1	6		6.6	0.05	
Anaerobic ammonia oxidation													
Amx_1	0.008	20	4	-	80	4	200	1	-	1	6.6	0.01	Kartel et al., 2012
Amx_2	0.004	0.5	1	-	0.5	1	50	1	-	1	6.6	0.01	

Table S2. Trait values used to initialize the different autotrophic functional guilds. Guilds represented include three groups of ammonia-oxidizing bacteria, three groups of nitrite-oxidizing bacteria, one group of ammonia-oxidizing archaea, and the groups of anaerobic ammonia oxidizers (anammox). Not all traits are represented in each functional guild

	Electron acceptor		
Electron Donor	Oxygen	Nitrate	Nitrous oxide
ED1	18.3	16.9	25.6
ED2	19.6	19.9	26.8
ED3	18.5	16.4	26.5

Table S3. Activity coefficients (given as Log(K_{eq})) associated with the $ED_{1,2,3}$ relative to different electron acceptors.

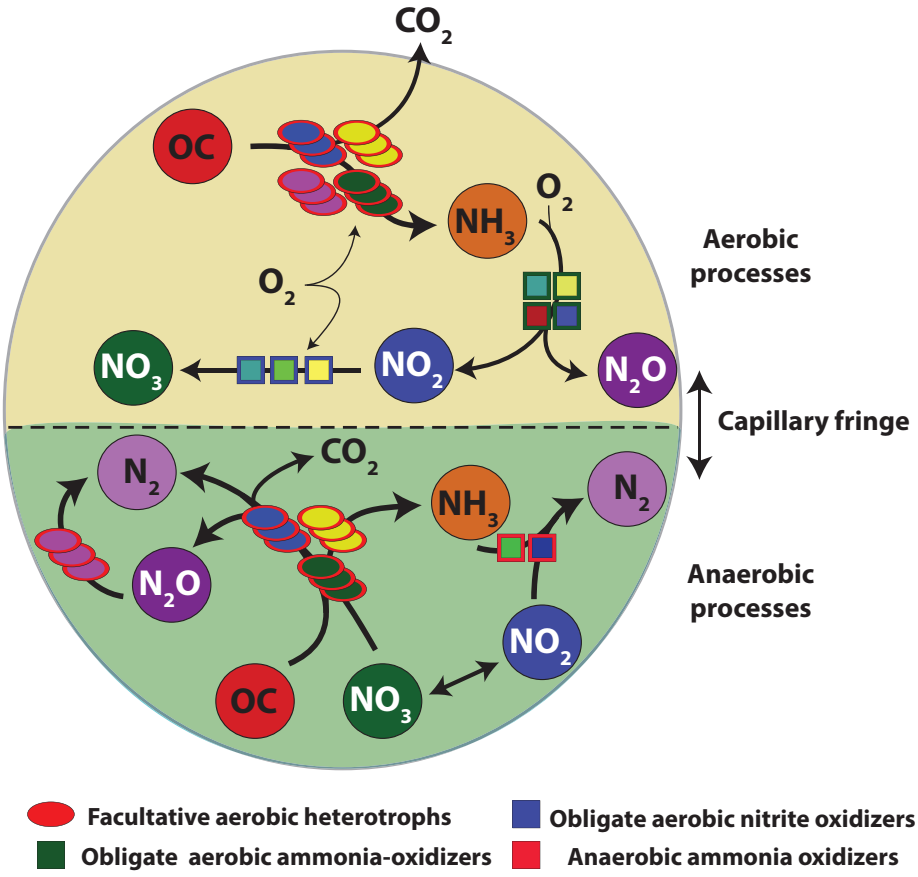

Figure S1. Model representation of interactions between autotrophic and heterotrophic guilds at the capillary fringe.

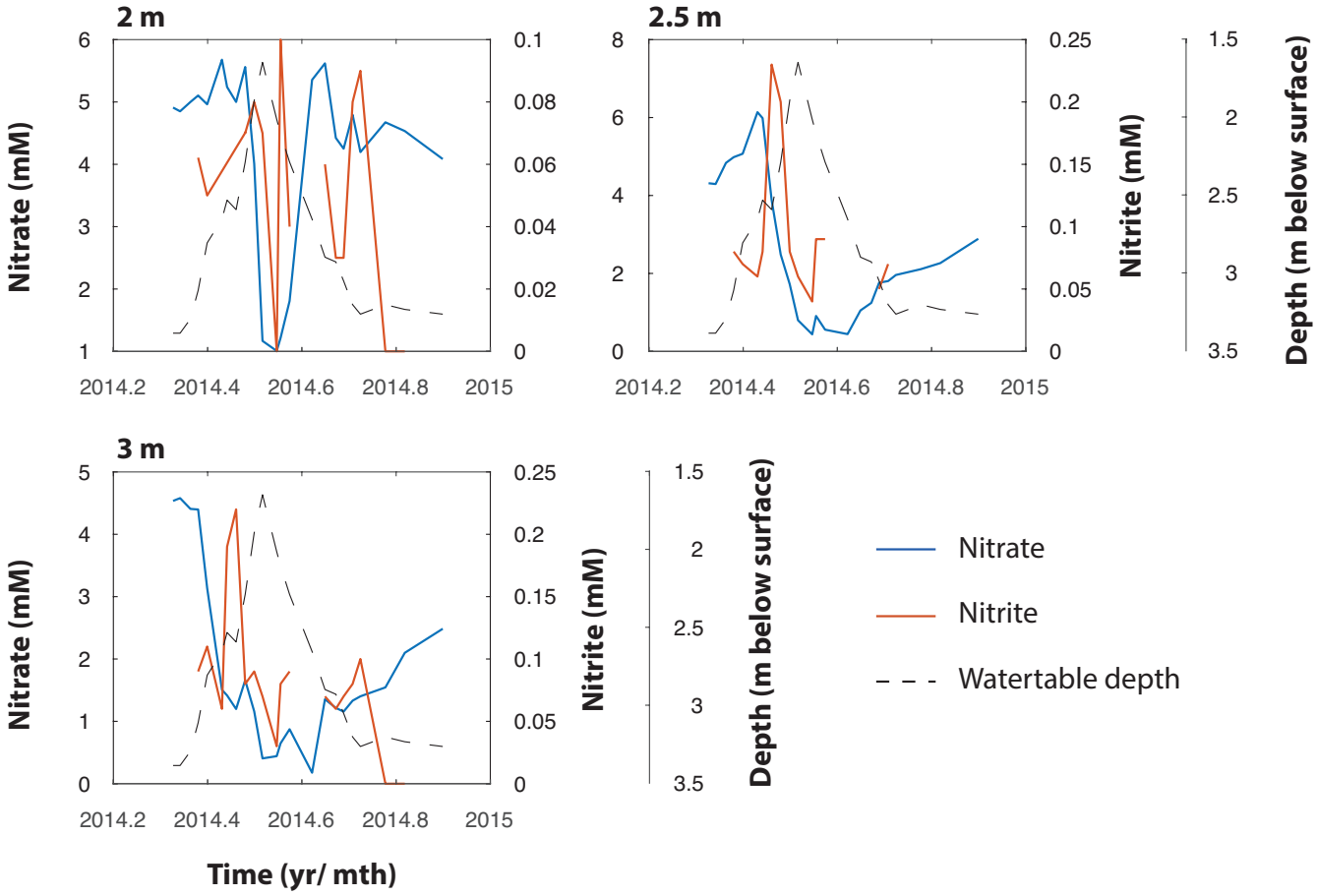

Figure S2. Nitrate (right axis) and nitrite (left axis) measurements at 2.0, 2.5 and 3.0 m bgs in TT-03 during 2014. The plots show coincidental and temporally lagged production of nitrite as nitrate declines, followed by apparent loss of nitrite. The water table depth is represented by the black dotted line.

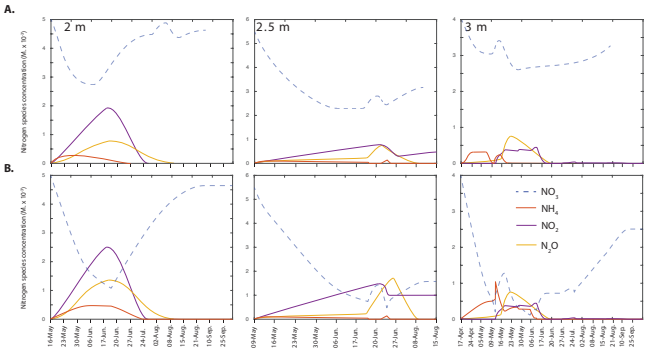

Figure S3. Geochemical output (NH_4^+, NO_2^-, NO_3^-, N_2O) from the microbial model at discrete depths and organic matter concentrations. A. Model response under OM concentrations typical of the aquifer (corresponding microbiological community response is given in Fig. 3 of the main text). B. Geochemical response under OM concentrations an order of magnitude higher than in A. Under these conditions microbial activity can account for all of the NO_3^- through denitrification.

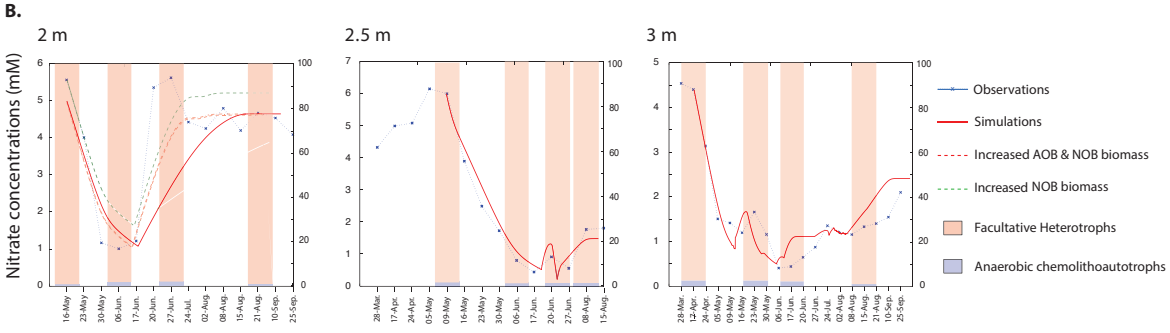

Figure S4. Microbiological community response under high OM concentrations (an order of magnitude higher than that in the main text). The corresponding geochemical response is given above (Fig. S3).

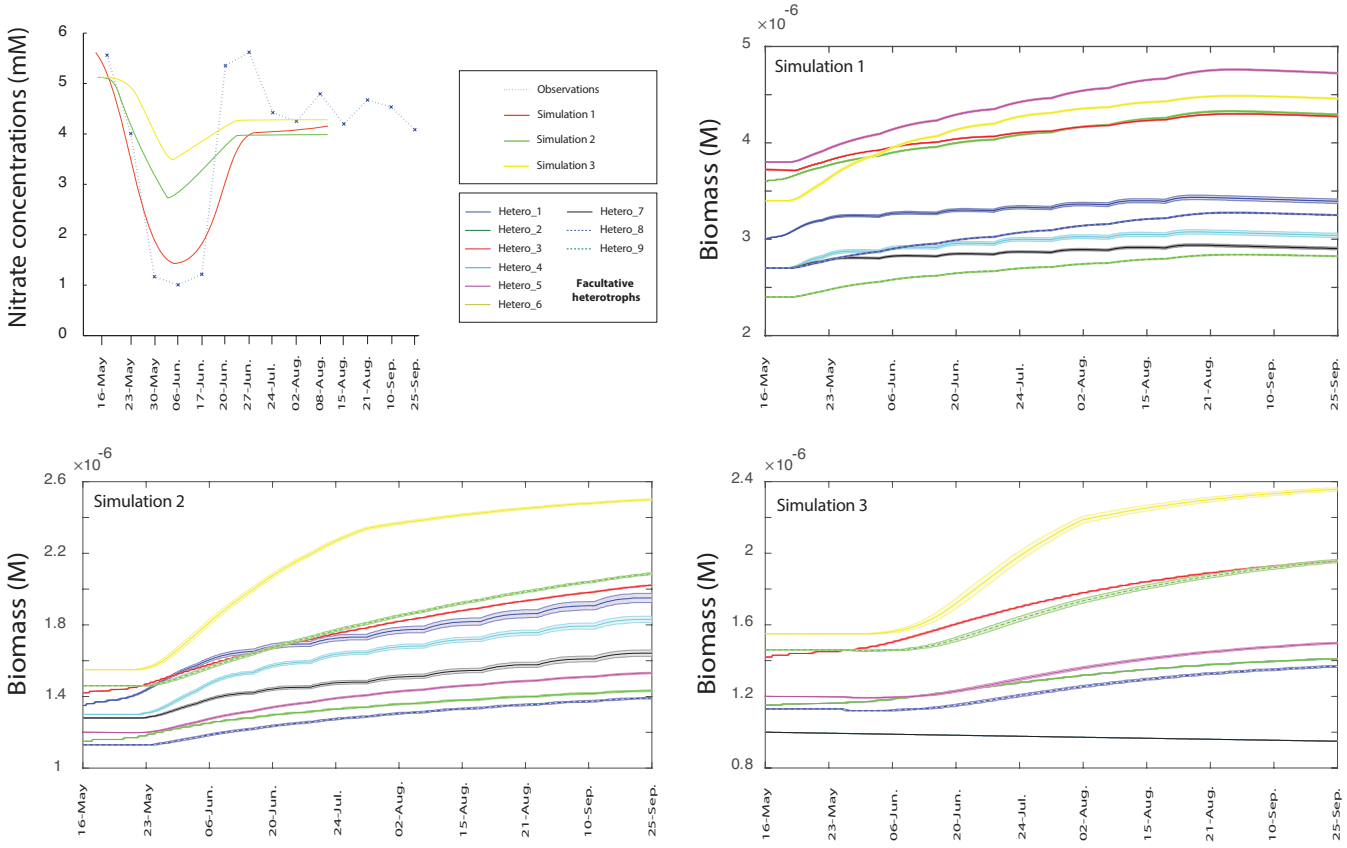

Figure S5. Heterotrophic community trajectory under different electron donor ratios. The relative ratios of ED_{1-3} was manipulated while maintaining the same concentration ($\sim$ 30 μM) pulsed at regular intervals. Simulation 1 represents the default simulation with $ED_{1,2,3}$ ratio of 50:25:25, simulation 2 increases the concentration of ED_3 to give a final ratio of 25:25:50, while the final simulation gives a splits the total OM concentration between ED_2 and ED_3 equally.

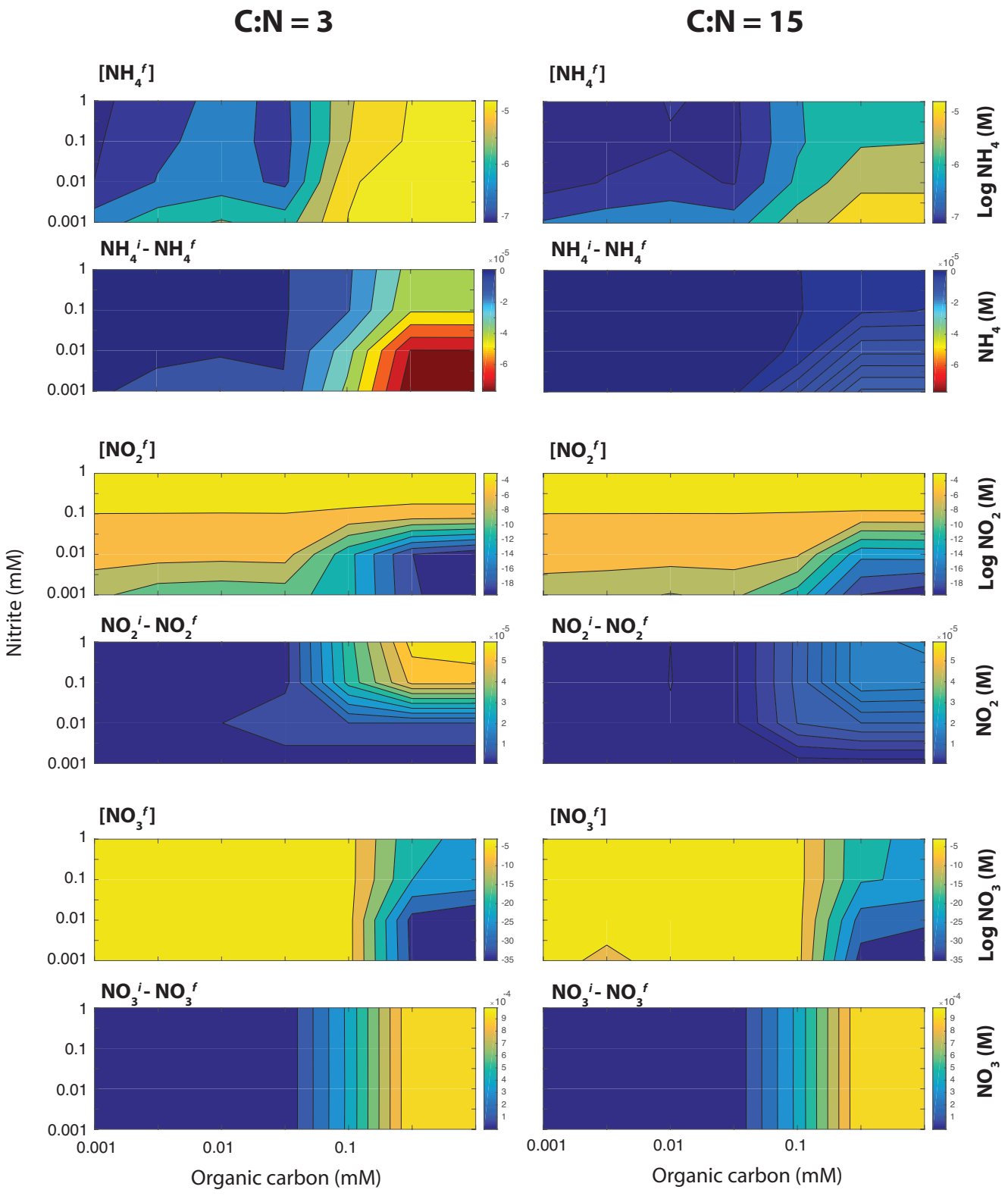

Figure S6. NH_4^+, NO_2^-, and NO_3^- distribution across gradients in NO_2^- and organic matter concentration at C:N ratios of 3 and 15. Panels show the final concentration of each species at the end of the simulation, and the difference between starting and finishing concentrations. The color differences in the NH_4^+ represents its accumulation.

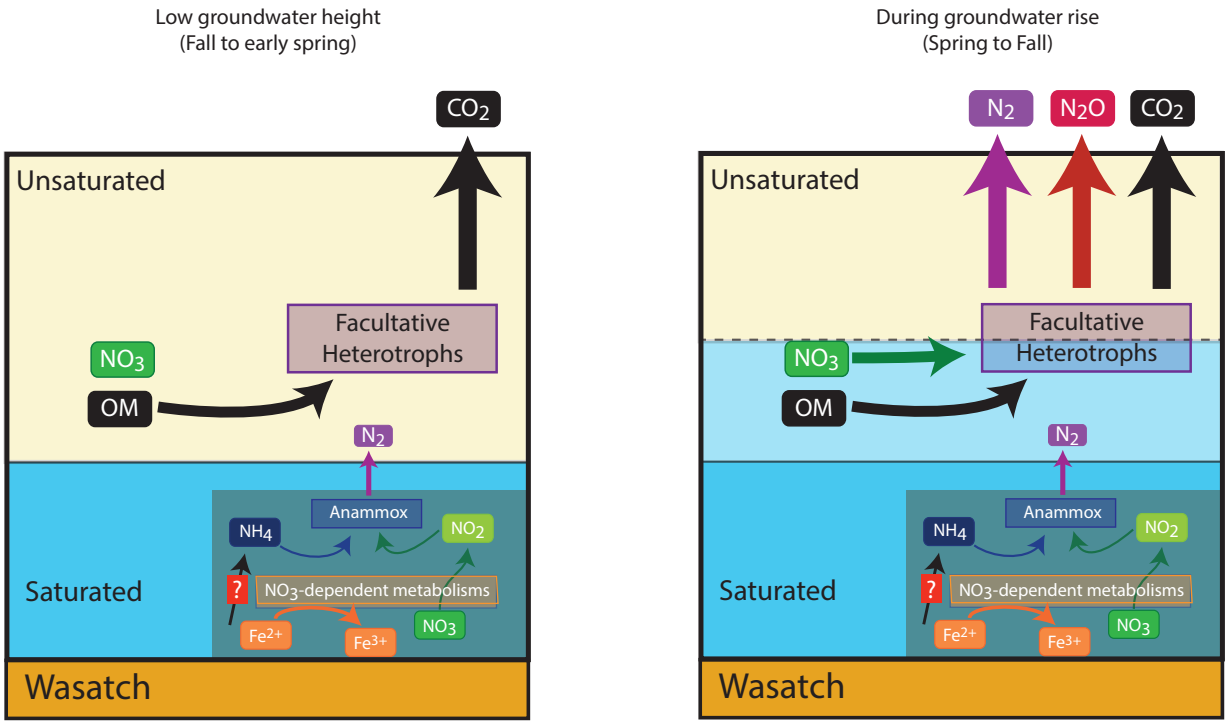

Figure S7. Conceptual nitrogen cycle within the Rifle aquifer on the basis of the measurements made in the present study, and recent molecular based studies.